Influence of *e-e* scattering on the temperature dependence of the resistance of a classical ballistic point contact in a two-dimensional electron system

M. Yu. Melnikov,[1] J. P. Kotthaus,[2] V. Pellegrini,[3] L. Sorba,[3] G. Biasiol,[4] and V. S. Khrapai[1]

[1]*Institute of Solid State Physics, Russian Academy of Sciences, 142432 Chernogolovka, Russian Federation*

[2]*Center for NanoScience and Fakultät für Physik, Ludwig-Maximilians-Universität, Geschwister-Scholl-Platz 1, D-80539 München, Germany*

[3]*NEST, Istituto Nanoscienze-CNR and Scuola Normale Superiore, Piazza San Silvestro 12, I-56127 Pisa, Italy*

[4]*CNR-IOM, Laboratorio TASC, Area Science Park, I-34149 Trieste, Italy*

We experimentally investigate the temperature (T) dependence of the resistance of a classical ballistic point contact (PC) in a two-dimensional electron system (2DES). The split-gate PC is realized in a high-quality AlGaAs/GaAs heterostructure. The PC resistance is found to drop by more than 10% as T is raised from 0.5 K to 4.2 K. In the absence of a magnetic field, the T dependence is roughly linear below 2 K and tends to saturate at higher T. Perpendicular magnetic fields on the order of a few 10 mT suppress the T-dependent contribution δR. This effect is more pronounced at lower temperatures, causing a crossover to a nearly parabolic T dependence in a magnetic field. The normalized magnetic field dependencies $\delta R(B)$ permit an empiric single parameter scaling in a wide range of PC gate voltages. These observations give strong evidence for the influence of electron-electron (*e-e*) scattering on the resistance of ballistic PCs. Our results are in qualitative agreement with a recent theory of the *e-e* scattering based T dependence of the conductance of classical ballistic PCs [Phys. Rev. Lett. **101**, 216807 (2008) and Phys. Rev. B **81**, 125316 (2010)].

PACS number(s): 73.23.−b, 73.23.Ad

I. INTRODUCTION

Electronic conductance of a diffusive solid-state system is characterized by a mean free path of charge carriers (l_0). Scattering off disorder and phonons, as well as electron-electron scattering (via U processes), contribute to a total quasimomentum relaxation rate, inversely proportional to l_0. With increasing temperature (T) the scattering typically becomes more effective and the mean free path decreases. The impact of scattering on the T dependence of the conductance differs in ballistic systems, among which a classical point contact is, perhaps, the simplest.

Introduced by Sharvin,[1] the classical ballistic point contact (PC) is represented by an orifice between two clean reservoirs with dimensions large compared to the inverse Fermi momentum (k_F). In two dimensions (2D), the conductance of the classical PC is given by a well-known analog of the Sharvin formula,[2]

$$G_0 = \frac{2e^2}{\hbar}\frac{ak_F}{\pi^2}, \qquad (1)$$

where e is the elementary charge, $\hbar$ is the Planck constant, and a is a half-width of the PC orifice, $ak_F \gg 1$. A finite mean free path in the reservoirs gives rise to a nonzero backscattering probability of the carriers injected through the PC. As a result, the PC conductance is smaller than the ideal value (1) roughly by $\delta G/G_0 \sim -a/l_0$. With increasing T the mean free path l_0 decreases and causes a negative T dependence of the PC conductance. Important in disordered systems, this effect can be neglected in contemporary high-quality devices ($a/l_0 \sim 1\%$), including those studied here.

In a recent work,[3] the impact of the *e-e* scattering on the conductance of classical PCs has been analyzed. As shown by the authors, the dominant contribution comes from scattering of the injected electrons with those incident onto the PC at large distances from the orifice. Contrary to naive expectations, this scattering mechanism *enhances* the conductance of the PC. For a classical PC in a two-dimensional electron system (2DES) with Fermi energy E_F and temperature T the *e-e* scattering contribution is found to be (the numerical factor is given after[4]),

$$\frac{\delta G_{ee}}{G_0} \approx 0.037\alpha_{ee}(ak_F)\frac{k_B T}{E_F}\ln(l_c/a), \qquad (2)$$

where $\alpha_{ee} \sim 1$ is a dimensionless *e-e* interaction parameter, k_B is the Boltzman constant, and $l_c \sim l_0 \gg a$ is a cutoff length scale in the 2DES. For a typical PC in a 2DES in GaAs the *e-e* scattering contribution is estimated as ∼10% at liquid He temperatures and, hence, expected to dominate the T dependence. More recently,[5] a suppression of the *e-e* scattering contribution to the PC conductance in small perpendicular magnetic fields has been calculated.

Ballistic constrictions in 2D have been extensively studied since the first observations of conductance quantization.[6,7] Thermal smearing of the conductance plateaus causes a well-known T-dependence mechanism in such devices.[8,9] A quantum-dot-Kondo-like T dependence in the region of the so-called 0.7 anomaly[10] is associated with many-body physics. *E-e* scattering-induced size effects in wide and long quasiballistic channels have been studied in Ref. 11. In those experiments, a current self-heating was used to vary the electronic temperature and a nonmonotonic behavior of the differential resistance was observed. The results were later interpreted as a 2D analog of a hydrodynamic-like Gurzhi effect.[12] A nonlocal hydrodynamic-like problem of electron injection through a PC was addressed in Ref. 13 in case of *e-e* scattering dominating all other scattering mechanisms. Corresponding experiments[14] have been performed in wide channels in a strongly nonlinear regime. Observation of the

e-e scattering contribution to the linear response Sharvin conductance requires careful measurements of the T dependence and magnetoresistance in PCs formed in a clean 2DES. We are aware of only one such experiment,[15] which is qualitatively consistent with the *e-e* scattering scenario of Refs. 3 and 5.

Here we present an experimental study of the T dependence of the resistance in split-gate-defined PCs in a GaAs-based 2DES at liquid He temperatures. In the absence of a magnetic field, a negative T-dependent resistance contribution on the order of 10% is found. The T dependence is suppressed by a small perpendicular magnetic field of a few 10 mT. The normalized magnetic field dependencies for different gate voltages obey an empiric single-parameter scaling procedure. The results give strong evidence for the influence of the *e-e* scattering on the PC conductance and are qualitatively consistent with the predictions of Refs. 3 and 5. We compare the measured functional dependencies on temperature and magnetic field with the theory predictions and discuss possible origins of the discrepancies, supported by a numerical calculation. In the absence of a magnetic field, a rough quantitative agreement is achieved and the interaction parameter α_{ee} is evaluated.

The paper is organized as follows. The experimental details are described in Sec. II. The results in zero and finite magnetic field are presented in Secs. III and IV, respectively. Section V is devoted to scaling of the magnetoresistance data. The discussion of the experimental results is given in Sec. VI. The details of the evaluation of the electron density inside the PC and those of numerical calculation are given in the Appendix A and B, respectively. The paper is briefly summarized in Sec. VII.

II. EXPERIMENTAL DETAILS

Our samples are based on a high-quality (001)GaAs/AlGaAs heterostructure containing a 2DES 200 nm below the surface. The electron density is about $n_S \approx 0.83 \times 10^{11}$ cm^{-2} (corresponding to $k_F \approx 7.2 \times 10^5$ cm^{-1}) and the mobility is $\approx 4 \times 10^6$ cm^2/Vs at $T = 4.2$ K, which corresponds to an elastic mean free path of ≈ 20 μm. The inset of Fig. 1(a) shows a micrograph of metallic split gates deposited on the crystal surface with the help of e-beam lithography (shown as two brighter areas). Negative gate voltages are applied to the gates in order to deplete the 2DES beneath them and define a PC. Throughout the paper, the voltage on the right gate is fixed at -0.4 V, while the left gate voltage (below simply gate voltage, V_g) can be varied to control resistance of the PC. Using a finite bias spectroscopy[16] we characterized a quasi-1D subband spacing ($\hbar\omega_\perp$) and a curvature of the PC potential along the transport direction ($\hbar\omega_\parallel$) in the spirit of a saddle-point model.[17] This was done in a device similar to the one for which the experimental data are presented below. The subband spacing decreases appreciably with the number of occupied 1D channels: from $\hbar\omega_\perp \approx 1.1$ meV for the 1-2 channels to ≈ 0.35 meV for the 5-6 channels. Respectively, the curvature along the transport direction decreases from $\hbar\omega_\parallel \approx 0.55$ meV to ≈ 0.35 meV. These parameters reflect the experimental observation that the fifth and higher conductance plateaus are hardly resolved even at very low T.[18] Consistently, the lithographic width of the PCs used is 260 nm, which gives
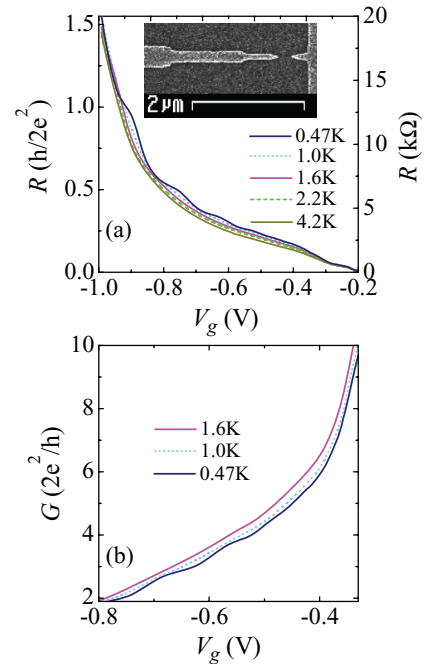

FIG. 1. (Color online) Gate-voltage dependencies of the PC resistance/conductance. (a) A four-terminal PC resistance for a set of temperatures in absolute (right axis) and dimensionless (left axis) units. (Inset) Electron micrograph of the surface of a sample analogous to that used in the experiment. Two top gates arranged in a T-shaped geometry appear in a light gray color. (b) A dimensionless PC conductance at the three lowest temperatures used in the experiment.

an upper bound of 6 for the number of quantized conductance plateaus.

The ohmic contacts to the electron system are obtained via annealing of Ni/Au/Ge/Ni/Au layers and placed at distances about 1 mm away from the PC. The experiment is performed in a ^{3}He insert at temperatures between 0.46 K and 4.2 K and in magnetic fields (perpendicular to the interface) up to 330 mT. The four-terminal resistance is measured with a lock-in amplifier with current excitation, ranging from 2 to 46 nA at frequencies between 12 and 32 Hz, strictly in the linear response. A 2DES resistance in series with the PC does not exceed 30Ω and has no impact on our results. The measurements were performed for a set of gate voltages fixed during a cool-down. The setup is equipped with a calibrated thermometer in the vicinity of the sample, which allowed us to measure the T dependence of the PC resistance during a slow (more than 1 h) cool-down or warm-up procedure. Rare random jumps in the resistance on the order of 1%, typically observed above 2 K [see Figs. 2(b) and 5(a)], are presumably caused by a nearby impurity recharging. When recording magnetic field dependencies, we compensated for these by a minor shift (<3%) of the curves in Fig. 3(b) such that the zero-field data points correspond to Fig. 2(b). Magnetic field sweeps exhibited a small hysteresis (less than ± 10 mT), which was accounted for with the help of Hall voltage measurements. Altogether we measured three PCs on two samples prepared from two similar wafers. The results are practically sample independent and reproducible in respect
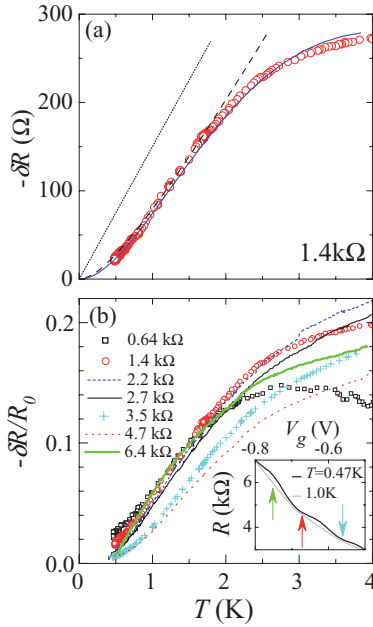
FIG. 2. (Color online) Temperature-dependent contribution to the PC resistance in the absence of a magnetic field. (a) Experimental T dependence for $R_0 \approx 1.4$ kΩ in absolute units (symbols). Model fits are shown by lines; see Sec. VI A. A fit according to Eq. (2) for $\alpha_{ee} = 0.77$, $a = 2 \times 290$ nm, and $l_c = 13$ μm is shown by a dotted line. A result of a numeric calculation in the spirit of Ref. 3 is shown by a dashed line for the same parameters. This fit is intended to describe deviations from a linear T dependence at low temperatures. The solid line demonstrates a numerical calculation which accounts for a beam decay effect due to *e-e* scattering. The parameters are $\alpha_{ee} = 1.75$, $l_c = 5$ μm, and the same a. (b) Normalized experimental T dependencies for a set of R_0 indicated in the legend. (Inset) Gate-voltage dependencies of the PC resistance for the two lowest temperatures. Arrows indicate the points where the three curves with high R_0 in (b) were taken.

to thermal recycling, so only the data for one PC obtained within the same thermal cycle are given below. Throughout the paper, with a few exceptions, we present the data for the PC resistance, which was actually measured in experiment. When comparing to theory, we make use of a relation between small contributions to the resistance and the conductance: $\delta R/R_0 = -\delta G/G_0$, with $R_0 = 1/G_0$.

III. PC RESISTANCE IN A ZERO MAGNETIC FIELD

Figure 1(a) shows gate-voltage dependencies of the PC resistance (R) for a set of T values. The traces start at $V_g = -0.2$ V, where (and at more positive V_g) the device resistance $\approx 30\Omega$ is dominated by that of the 2DES connected in series. At more negative gate voltages, the 2DES below the left gate depletes. Note that the gate metallization consists of three parts of different widths [inset of Fig. 1(a)], with the width sometimes being smaller than the distance to the 2DES layer. That is why the 2DES depletion under the gate occurs within a relatively wide range -0.22 V $< V_g < -0.35$ V, where three successive steps on the dependencies $R(V_g)$ can be resolved in Fig. 1(a). Below $V_g \approx -0.35$ V all the current flows through the PC constriction formed in the 2DES. The physical width
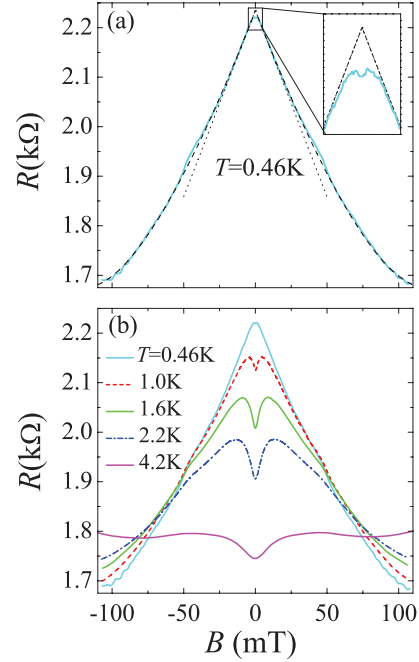

FIG. 3. (Color online) Magnetoresistance of the PC for $R_0 \approx 2.2$ kΩ. (a) Experimental dependence $R(B)$ for the lowest accessible T (solid line) and the fits accounting for the suppression of backscattering in $B \neq 0$ (dotted line) and, additionally, for the magnetoelectric subband depopulation (dashed line). (Inset) Magnified low-B region of the main figure with dimensions 45 $\Omega \times$ 10 mT. The experimental data in the inset (solid line) are obtained in a separate low-B sweep with a better resolution. The fits in (a) are obtained assuming the electron densities of 8.3×10^{10} cm^{-2} and 3.15×10^{10} cm^{-2}, respectively, in the 2DES and inside the PC. The deduced R_0 equals 2235 Ω. (b) Evolution of the experimental magnetoresistance with temperature.

of the PC, as well as the electron density inside it, is tuned by stray electric fields, such that its resistance increases towards more negative V_g. Within the range -0.5 V $< V_g < -0.35$ V the gate-voltage dependencies are featureless and the device behaves as a classical PC with the resistance $0.24h/2e^2 > R > 0.12h/2e^2$ (corresponding to 3.1 k$\Omega > R > 1.5$ kΩ). In order to cover a broader resistance range, we also performed the experiment outside this gate-voltage interval. At more negative gate voltages, -0.8 V $< V_g < -0.5$ V, we enter a quantum PC regime at the lowest T and study the PC resistances up to $R \approx 6.4$ kΩ ($0.5h/2e^2$). At more positive gate voltages, -0.35 V $< V_g < -0.27$ V, the PC constriction is not yet fully developed and its width exceeds the lithographic one. Here, PC resistances down to $R \approx 0.64$ kΩ ($0.05h/2e^2$) are accessible. As seen already from Fig. 1(a), the negative T-dependent contribution is found within the whole resistance range studied.

The effect of a finite temperature is easier to observe in the gate-voltage dependence of the PC conductance $G = 1/R$. This is shown in Fig. 1(b) for a relevant V_g range at the three lowest experimental temperatures. At the lowest $T \approx 0.47$ K the signatures of the quantized plateaus $2ne^2/h$ ($n = 2,3,4$) are resolved. The impact of increasing T is twofold: It causes (i) a smearing of the plateaus and (ii) an overall conductance increase. The first effect is caused by a well-known thermal

broadening[8] of the Fermi distribution function. However, as Fig. 1(b) demonstrates, at temperatures above 1 K the gate-voltage dependencies of the conductance are already smooth, and this effect has a minor (if any) contribution to the T dependence. In what follows, we focus on a second effect: the pronounced positive/negative T dependence of the conductance/resistance, which is similar to the results of Ref. 15 and observed within the whole gate-voltage interval in Figs. 1(a) and 1(b). This effect dominates the T dependence above 1 K.

In Fig. 2(a) the T dependence of the PC resistance is shown for $V_g = -0.337$ V (symbols). The data are plotted in the form of a T-dependent contribution $-\delta R \equiv -[R(T) - R_0]$, where $R(T)$ is the measured resistance at a given temperature. The resistance R_0, which determines the absolute value of the T-dependent contribution, is deduced from the magnetoresistance data of Sec. IV. The overall T dependence of the PC resistance in Fig. 2(a) is negative such that $-\delta R$ monotonously increases with increasing temperature. The T dependence is strongest for 1 K $< T <$ 2 K, where $-\delta R$ increases by a factor of 2.3 almost linearly with T. At higher temperatures, the T dependence becomes substantially weaker and $\delta R(T)$ tends to saturate. Since $\delta R(T = 0) = 0$, the data imply that the T dependence should also weaken at $T \to 0$. Yet temperatures used are not low enough for this tendency to be pronounced in Fig. 2(a).

Similar qualitative behavior is observed in a wide range of gate voltages, as shown in Fig. 2(b). Here the relative contribution $-\delta R/R_0$ is plotted as a function of T for a set of PC resistances, 0.64 k$\Omega \leqslant R_0 \leqslant 6.4$ kΩ. Again, the negative T dependence is strongest at intermediate T, and weakens at high and low T, with some minor differences. For instance, the lowest resistance trace ($R_0 = 0.64$ $k\Omega$) demonstrates a high-T downturn, which seems to have the same origin as the saturation of the T dependencies for higher R_0 (see Sec. VI A). At $T < 1$ K the three traces with high R_0 suffer from a residual thermal smearing of the $n = 2, 3, 4$ resistance plateaus. This effect contributes a spurious positive (negative) T dependence on the low-V_g (high-V_g) edge of a resistance plateau.[8] As a result, below 1 K the measured T dependence is stronger for the 6.4-kΩ trace and weaker for the 4.7-kΩ and 3.5-kΩ traces; see the inset of Fig. 2(b).

The data of Fig. 2 demonstrate a negative T dependence of the PC resistance on the order of $\sim$10% at liquid He temperatures. This effect is observed in a wide range of resistances from the limit of classical PC ($R_0 \ll h/2e^2$) to the quantum PC regime (up to $R_0 \approx 0.5 h/2e^2$). The negative T dependence of the resistance cannot be interpreted in terms of a backscattering of electrons due to a finite elastic mean free path in the 2DES. In our ballistic PC, the overall backscattering contribution is too small (on the order of $a/l_0 \sim 1\%$) and would result in a positive T dependence of the resistance. One can also safely neglect a possible contribution from the weak localization in the 2D leads, which results in a negative T-dependent contribution several orders of magnitude smaller than that in Fig. 2. Instead of single-particle effects, we attribute the T dependence of the PC resistance to the e-e scattering scenario,[3] which turns out to be consistent with the results of the experiment (see Sec. VI). The behavior of the magnetoresistance data in small perpendicular magnetic

fields, presented in the next section, further support this hypothesis.

IV. PC RESISTANCE IN A PERPENDICULAR MAGNETIC FIELD

In Fig. 3(b) the experimental PC magnetoresistance is plotted for a set of temperatures at a gate voltage of $V_g = -0.41$ V, corresponding to a classical PC regime. In small fields, the curves $R(B)$ demonstrate a negative T dependence. The dependence is strongest at $B = 0$ and quickly suppressed with increasing magnetic field. As a result, a pronounced zero-field resistance minimum is observed, which becomes wider and deeper as T is raised. The T-dependent magnetoresistance is well seen even for $|B| < 10$ mT, where the cyclotron radius ($R_C > 4$ μm) by far exceeds the size of the PC orifice. This observation gives a strong evidence that the T-dependent PC magnetoresistance originates from the neighboring 2DES in agreement with the e-e scattering scenario.[5] In higher magnetic fields $|B| \gtrsim 50$ mT a sign change of the T dependence is observed in Fig. 3(b) (signatures of such a behavior were also seen in Ref. 15), which we failed to unambiguously interpret. For this reason, in the following we limit our analysis to the magnetic field range $|B| \leqslant 25$ mT.

Before analyzing the T-dependent contribution in detail, we note that in Fig. 3(b) it is superimposed on a well-known single-particle magnetoresistance[19] (see also Ref. 5). The latter contribution is independent of T and can be identified in the low-T limit. In Fig. 3(a) the PC resistance at the lowest $T \approx 0.47$ K is plotted as a function of B (thick line) for the same V_g as in Fig. 3(b). The overall magnetoresistance is negative and well explained by two single-particle effects. The first contribution results from a nonadditivity of the ballistic PC resistance and Hall resistance $R_H = B/(ecn_S)$ of the neighboring 2DES leads (so-called suppression of backscattering[20]). In a quasiclassical approximation,[19] the four-terminal PC resistance exhibits a negative linear magnetoresistace $\delta R(B) = -|R_H| \propto -|B|$. As seen from Fig. 3(a), for $|B| \leqslant 25$ mT the experimental magnetoresistance has the same slope as that of $-|R_H|$ (dots) with a value of n_S deduced from Shubnikov oscillations in the bulk 2DES. In stronger magnetic fields, the experimental magnetoresistance weakens, due to a second effect—namely, depopulation of magnetoelectric subbands in the PC.[19] To the lowest order in B, this effect contributes a positive magnetoresistance $\propto B^2$. As shown in Fig. 3(a), taking both these contributions into account results in a nearly perfect fit (dashed line) to the experimental curve for $|B| \leqslant 100$ mT. Hence, other possible B-dependent contributions (including e-e scattering[5]) are negligible at this temperature, except for a tiny field range magnified in the inset of Fig. 3(a).

In the inset of Fig. 3(a), the experimental magnetoresistance is shown along with the fits of Fig. 3(a) extrapolated towards $|B| \to 0$. At $B = 0$, the single-particle extrapolation predicts a resistance slightly higher than actually measured. In part, this deviation is caused by a rounding of the sharp $B = 0$ kink in a real 2DES.[21] However, a tiny region of very weak positive magnetoresistance seen in the inset of Fig. 3(a) suggests that at the lowest temperature used the T-dependent contribution survives for $|B| < 3$ mT and contributes to the deviation from
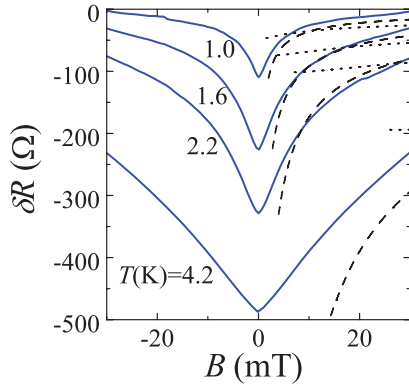
FIG. 4. (Color online) Magnetic field suppression of the T-dependent contribution to the PC resistance. Experimental data [obtained from Fig. 3(b), see text] are shown with solid lines. The best fit with Eq. (3) (parameters $\alpha_{ee} = 0.3$, $a = 204$ nm, $R_0 = 2235$ Ω with an assumed density inside the PC 3.15×10^{10} cm^{-2}) and the empiric fit $\delta R_{ee} \propto T^2 |B|^{-0.7}$ are shown with a dotted and dashed line, respectively.

the extrapolated single-particle fits. This deviation being small ensures that the complete fit to the lowest T magnetoresistance data (dashed line in Fig. 3(a)) can serve as a reliable $T \to 0$ limit.[22] This fit is used as a reference curve $R^{\mathrm{REF}}(B)$ to determine the T-dependent contribution $-\delta R(B,T) = R^{\mathrm{REF}}(B) - R(B,T)$, where $R(B,T)$ is the measured resistance at a given magnetic field and temperature. In a zero field we have $R_0 \equiv R^{\mathrm{REF}}(B=0)$. The same procedure is used at every gate-voltage value. All such fits are performed with the same Hall coefficient, corresponding to the bulk 2DES density. The subband depopulation effect in each case is fitted separately in a hard-wall model with an electron density inside the PC as a fit parameter (Appendix A). A possible systematic error ($<1\%$ in the classical PC regime) in chosen $R^{\mathrm{REF}}(B)$ is not important as long as $|\delta R|/R_0$ is not too small, i.e., for $T \geqslant 1$ K and in not-too-high magnetic fields. Note that in the quantum PC regime such a procedure does not allow us to overcome the T dependence due to the smearing of the resistance plateaus, which is independent of magnetic field. Hence, the systematic error is higher in that case and on the order of a few percentages.

In Fig. 4 the B dependencies of $\delta R(B,T)$, obtained from the data of Fig. 3(b) as described above, are plotted for a set of temperatures. The absolute value $|\delta R|$ exhibits a maximum at $B = 0$, symmetric with respect to field reversal and decays in magnetic field. The functional B dependence weakens as the magnetic field is increased. Dashed lines in Fig. 4 show the best empiric power law fit to the experimental data set with an expression $\delta R \propto -T^2 B^{-0.7}$. We find such a fit reasonable at intermediate temperatures $T \leqslant 2.2$ K except for small $|B|$. Scaling of the magnetoresistance data at different V_g (Sec. V) indicates that similar functional B dependencies $-\delta R(B)$ are observed in a wide range of the PC gate voltages.

In Fig. 5(a) the measured T dependencies are plotted for a set of fixed (positive) B values. At $B = 0$, as discussed above, a nearly linear T dependence is observed for $T < 2$ K, followed by saturation at higher T. The B-driven suppression of the T-dependent contribution is stronger at lower T. As a result,
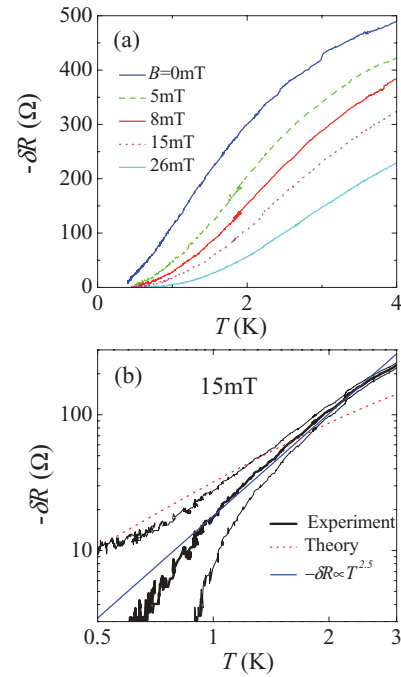

FIG. 5. (Color online) Evolution of the T dependence with magnetic field for $R_0 \approx 2.2$ kΩ. (a) Experimental T dependencies plotted in linear scale for a set of magnetic field values. (b) Double-log plot of the experimental dependence at $B = 15$ mT (thick solid line), together with the fit to Eq. (3) (parameters $\alpha_{ee} = 0.3$, $a = 204$ nm, $R_0 = 2235$ Ω with an assumed density inside the PC 3.15×10^{10} cm^{-2}) and the empiric dependence $\delta R \propto -T^{2.5}$. Thin solid lines indicate the range of possible systematic uncertainty associated with the choice of R_0. These lines are obtained via shifting the thick solid line by ± 10 Ω.

with increasing B the T dependence approaches parabolic at low temperatures.

For a quantitative analysis of the T dependence we plot the data at $B = 15$ mT on a double logarithmic scale in Fig. 5(b) (thick solid line). The experimental uncertainty is indicated as follows. The reference value $R^{\mathrm{REF}}(B)$ is determined with an accuracy of ± 10 Ω, appreciably worse than the random error in a measured T dependence (± 2 Ω). This unknown additive contribution to $\delta R(T)$ could shift the data up or down as a whole to a position somewhere between those indicated with thin solid lines in Fig. 5(b). Within this uncertainty, the experimental data are compatible with a power-law $\delta R(T) \propto -T^\alpha$, where $\alpha \approx 2.5 \pm 0.5$. The best such fit $-\delta R \propto T^{2.5}$ is shown by a thin solid line in Fig. 5(b).

The key experimental observations of Figs. 3, 4, and 5 can be qualitatively explained in the framework of the *e-e* scattering contribution to the PC resistance. As predicted in Ref. 5, the *e-e* scattering is suppressed by a perpendicular magnetic field $B \neq 0$, as a result of time-reversal symmetry breaking. A typical B-field scale (a few 10 mT) is defined by competition of an interaction time argument[5] and phase-space constraints and increases with T. The corresponding magnetoresistance contribution is positive and T dependent. It is predicted to be observable already in tiny magnetic fields, where the cyclotron radius in the 2DES $R_C = \hbar k_F c / eB$ is much larger than the size of the orifice,[5] in perfect agreement with our experiment. We

next demonstrate that the magnetoresistance data are similar in a wide range of the PC gate voltages (i.e., R_0), permitting a single parameter scaling.

V. SCALING THE MAGNETORESISTANCE DATA AT DIFFERENT GATE VOLTAGES

In Fig. 6(a) we compare the curves $\delta R(B)$ taken at $T = 1.6$ K for two different V_g corresponding to the PC resistances of $R_0 \approx 1.4$ kΩ and $R_0 \approx 3.4$ kΩ. In both cases, the overall effect of magnetic field is qualitatively similar to that in Fig. 4 and the absolute value $|\delta R(B)|$ increases with R_0. At the same time, the width of the V-shaped dependence along the B axis also increases with R_0, as demonstrated by arrows in Fig. 6(a), which mark the full width at the half minimum $\delta R(B)$. This behavior is observed within the whole range of R_0 investigated and for all T used.

We find that the data $\delta R(B)$ at different R_0 permit a single parameter scaling. At a given T, an empiric relation $a_{\text{eff}}^{-1} \delta R/R_0 \approx F(a_{\text{eff}} B)$ holds, where a_{eff} is an R_0-dependent scaling parameter and F is a function which determines the shape of the B dependence at this T. It is convenient to express a_{eff} in units of length and plot the scaled B dependencies in dimensionless coordinates $\delta R/R_0 \times w/a_{\text{eff}}$ vs $\beta \equiv a_{\text{eff}}/R_C$, where $w = 130$ nm is the lithographical half-width of the PC and $R_C \propto B^{-1}$ is the cyclotron radius in the 2DES. This choice of axes is natural for the e-e scattering mechanism of the T dependence, as explained in Sec. VI.
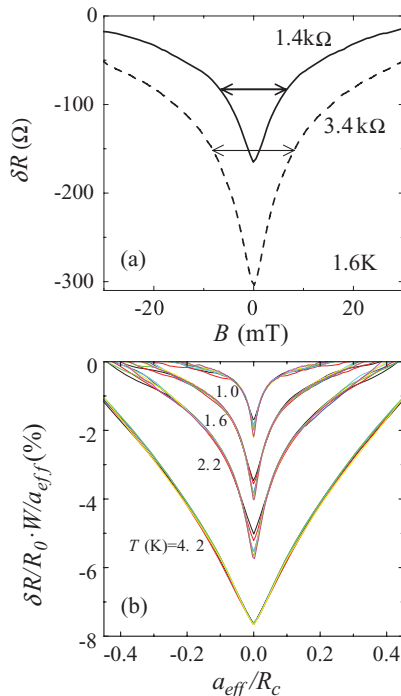

FIG. 6. (Color online) T-dependent contribution to the magnetoresistance at different R_0. (a) Experimental dependencies $\delta R(B)$ for two values of R_0 at 1.6 K. The arrows mark the full width at the half minimum of the V-shaped dependencies. (b) One-parameter scaling of the magnetoresistance data for $R_0 \leqslant 6.4$ kΩ. The temperature increases from top to bottom $T = 1, 1.6, 2.2, 4.2$ K.
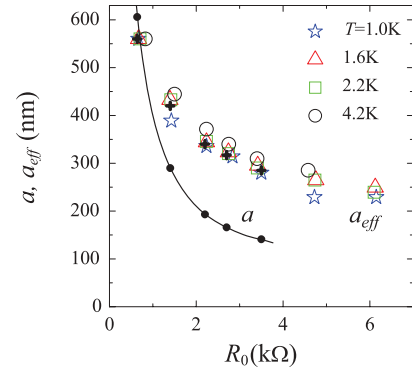

FIG. 7. (Color online) Dependence of the scaling parameter a_{eff} from Fig. 6 (symbols) and the physical half-width a of the PC (line) on R_0. The physical half-width a is evaluated from Eq. (1) with $G_0 = 1/R_0$, with a reduced electron density inside the PC taken into account (see Appendix A). The scaling parameter a_{eff}, normalized as described in the text, is shown by separate symbols for the four temperatures used. Black dots and crosses mark, respectively, the values of a and a_{eff} used in numerical fits; see Appendix B.

In Fig. 6(b), we plot the results of the scaling procedure for a wide range of R_0. For each of the four temperatures used, the data are obtained as follows. We vary the value of a_{eff} such that the dependencies $\delta R(B)/R_0$ at different R_0 fall on a single curve. For better scaling, the value of R_0 is also slightly varied within the experimental uncertainty (a few percentages). Note that the values of R_0 are consistent with the $T = 0.47$ K data[18] and are not expected to exhibit clear resistance quantization effects for the reasons discussed above (see Sec. IV). At a given T, a nearly perfect scaling is obtained in the region of not-too-high $|\beta|$, where $\delta R(B)/R_0$ is not small, and outside the very vicinity of $\beta = 0$ (i.e., zero magnetic field). The scaling is successful even far from the classical PC limit, up to $R_0 \approx 0.5h/2e^2$. Remarkably, a similar low-B behavior is observed even close to the resistance quantum h/e^2, although the scaling is worse for such high R_0 (not shown).

In Fig. 7 we plot the scaling parameter a_{eff} (symbols) as a function of R_0. The absolute value of a_{eff} is not determined in a scaling procedure and is chosen to coincide with the physical half-width a of the PC on the lowest R_0 end. Normalized in this way, a_{eff} is nearly T independent and decreases at increasing R_0. As seen from Fig. 7, a_{eff} drops by less than a factor of 3 when R_0 is varied by almost an order of magnitude.

VI. DISCUSSION

As demonstrated in previous sections, the resistance of a ballistic PC in a high-quality 2DES exhibits a negative T dependence at liquid He temperatures. In the absence of magnetic field, the T dependence is relatively strong below $T \approx 2$ K and tends to saturate at higher temperatures. At not too high T, a small magnetic field on the order of a few 10 mT tends to suppress the T dependence. These observations can be well explained in terms of the e-e scattering contribution to the ballistic PC resistance. The experimental data are qualitatively consistent with the predictions of the theory of Refs. 3 and 5 for classical PCs, which is the only present theory capable to closely describe the data. Below we discuss

the experimental results in detail, quantitatively compare the experimental behavior with key theoretical predictions, and attempt to evaluate the strength of the *e-e* scattering in the 2DES studied.

A. Zero magnetic field

1. Qualitative picture at not-too-high T

At temperatures in the range 0.5 K $< T \lesssim 2$ K, the experimental T dependence of the resistance is not far from linear [see symbols Fig. 2(a)]. Still, at low T the dependence is incompatible with the proportionality $|\delta G_{ee}| \propto T$ predicted by Eq. (2). This is strongly supported by the magnetoresistance data of Sec. IV, where the contribution of *e-e* scattering is almost negligible at the lowest temperature used $T \approx 0.5$ K. This behavior is captured by a numerical calculation of the *e-e* scattering contribution in spirit of Ref. 3 (see Appendix B for the details) and can be qualitatively understood as follows.

Consider a scattering of an injected electron (momentum **k**) with the one incident onto the PC (momentum **p**) at large distances r from the orifice ($r \gg a$). The two momenta are approximately opposite such that the angle φ between **k** and $-$**p** is small: $|\varphi| \lesssim \phi_{PC} \ll 1$, where $\phi_{PC} = a/r$ is the angular dimension of the PC orifice at a distance r. For $|\varphi| \lesssim \phi_T$ (with a thermal angle defined as $\phi_T \approx T/E_F$), the two electrons can scatter by an arbitrary angle[12] and the scattering probability is independent of φ. Outside this range, for $|\varphi| > \phi_T$, the scattering probability decreases with increasing $|\varphi|$ and, accordingly, the scattering angle cannot exceed $\sim \phi_T/|\varphi|$. These constraints result from the conservation laws and the Pauli principle. Depending on T and/or r, two limiting cases can be realized.

Figure 8 sketches the momentum space for the two limiting cases. A situation of Fig. 8(a) is realized when $\phi_{PC} < \phi_T$, i.e.,
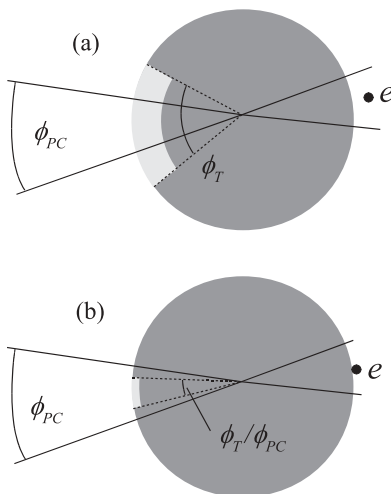

(a)

ϕ_{PC}

ϕ_T

$\bullet e$

(b)

ϕ_{PC}

ϕ_T/ϕ_{PC}

$\bullet e$

FIG. 8. A sketch of momentum space in the 2DES at a distance $r \gg a$ from the orifice for two limiting cases of not too low T (or large r: $\phi_T \gg \phi_{PC}$) (a) and very low T [or small r: $\phi_T \ll (\phi_{PC})^2$] (b); see text. A typical state of a nonequilibrium electron injected through the PC is shown by a black dot. The dark gray color indicates occupied states below the Fermi surface. Electron states with approximately opposite momenta available for *e-e* scattering are shown as light gray areas (see text for the details).

at not-too-low T (and/or not too small r). In this case, an average injected electron (shown by a black dot) can scatter by an arbitrary angle with each of the electrons within the stripe $|\varphi| < \phi_T$ of the width $\sim T$ (shown by a light gray color). However, only the scattering with the electrons within the angle $|\varphi| \lesssim \phi_{PC}$ can contribute to the PC conductance. Hence, $\delta G_{ee} \sim \phi_{PC} \times T$, which, in the end, gives rise to the linear T dependence and a log dependence on l_c in Eq. (2), derived in Ref. 3. At $T \to 0$ the condition $\phi_{PC} < \phi_T$ breaks down and one expects deviations from the linear T dependence. In Fig. 8(b) we sketch a situation in the limit of very low T such that $\phi_T \ll (\phi_{PC})^2$. Here an average injected electron (black dot) cannot effectively scatter an incident electron unless $|\varphi| \lesssim \phi_T/\phi_{PC}$. The corresponding momentum space region of width $\propto T$ is shown by a light gray color in Fig. 8(b). Outside this region, for larger $|\varphi|$, the typical scattering angle is smaller than ϕ_{PC}. Corresponding scattering processes do not influence the conductance for one of the scattered electrons still reaches the PC orifice. In this limit the *e-e* scattering contribution acquires a parabolic[23] T dependence $\delta G_{ee} \propto T^2$.

The dashed line in Fig. 2(a) represents a numerical fit to the experimental data (symbols) performed in the framework of Ref. 3. The calculation exhibits a crossover between the two limiting cases considered above and is quantitatively consistent with the experiment at $T \lesssim 2$ K for the chosen fit parameters (see caption). For comparison, the dependence predicted by Eq. (2) for the same fit parameters is shown by the dotted line in Fig. 2(a). Note that the numerically calculated T dependence is strongly nonlinear below 0.5 K. This demonstrates that a naive linear extrapolation of the experimental dependence $R(T)$ towards $T = 0$ may be misleading and an independent determination of R_0 is needed (see Sec. IV). The low-T behavior is related to the value of the cutoff length l_c, which is expected to be comparable to the elastic mean free path.[3] As discussed in Appendix B, at increasing l_c the numerical result asymptotically approaches the analytic prediction of Eq. (2) for arbitrarily low temperatures. Hence, a proportionality[3] $\delta G^{ee} \propto T$ might be observed in samples of exceptionally high quality in future (see Appendix B).

2. High-T behavior and beam decay effects

As seen from Fig. 2(a), the experimental T dependence levels off and tends to saturate at $T > 2$ K. A similar behavior $\delta R(T)$ is observed within the whole range of gate voltages studied [Fig. 2(b)], which is not predicted by theory.[3] We find that such a qualitative behavior is in fact expected for the *e-e* scattering scenario at high-enough T and is related to a breakdown of a condition $l_c \ll l_{ee}$, where l_{ee} is an electron mean free path for *e-e* scattering. In such a situation, a decay of the injected beam on the length scale of l_c due to the *e-e* scattering is not negligible. Therefore, the total *e-e* scattering probability is no longer small and the calculations[3] to first order in α_{ee} are expected to overestimate the effect of *e-e* scattering on the PC conductance.

One can estimate the length l_{ee} based on a calculation of a quasiparticle lifetime.[24] This calculation agrees with energy-relaxation data in a high-density device.[26] In our 2DES at $T = 4$ K such an estimate gives $l_{ee} \approx 2.7 \ \mu$m, indeed much smaller than the elastic mean free path l_0. Moreover,

we estimate that the condition $l_0 \sim l_c \ll l_{ee}$ is satisfied only at $T \ll 2$ K. Therefore, the applicability range of the numeric calculation in spirit of Ref. 3 turns out to be too narrow for a reliable estimation of the *e*-*e* interaction parameter α_{ee}. Unfortunately, a mathematically strict account for the effects of the beam decay due to *e*-*e* scattering is too involved for modeling. Nevertheless, we performed additional numerical calculations with an *ad hoc* introduced decay of the injected beam with characteristic length scale of l_{ee}. These calculations are capable of reproducing the *T* dependence in the whole temperature range studied; see Appendix B. One such fit perfectly consistent with the experiment is plotted by a solid line in Fig. 2(a). Note that the interaction parameter α_{ee} obtained from such fits is roughly 2 times larger compared to the fit in which the beam decay effect is disregarded [dashed line in Fig. 2(a)].

B. Finite magnetic field

Thanks to the time-reversal symmetry breaking, the contribution of the *e*-*e* scattering to the PC conductance is expected to rapidly decay in a perpendicular magnetic field.[3] The theoretical prediction of Ref. 5 for not-too-small magnetic fields is given by

$$\frac{\delta G_{ee}}{G_0} = \frac{2}{9}\alpha_{ee}\frac{ak_F}{\sqrt{\beta}}\frac{k_B^2 T^2}{E_F^2}\ln\left(\beta\frac{E_F^2}{k_B^2 T^2}\right). \tag{3}$$

This result is derived assuming $k_B^2 T^2/E_F^2 \ll \beta \ll 1$, where $\beta \equiv a/R_C \propto B$ is the ratio of the half-width of the PC orifice to the cyclotron radius in the 2DES $R_C = \hbar k_F c/eB$.

Equation (3) predicts that a decay of δG_{ee} in a perpendicular magnetic field causes a *T* dependence stronger than that at $B = 0$. On the other hand, as follows from this expression, at higher temperatures a decay of δG_{ee} occurs in stronger magnetic fields scaling as $\sqrt{\beta} \propto T$. This behavior has to do with the physics of *e*-*e* scattering in a perpendicular magnetic field. Quasiclassically, the *e*-*e* scattering probability is proportional to the effective interaction time between the scattering electrons. The interaction time depends on the angle φ between the momenta **k** and $-\mathbf{p}$ (defined in Sec. VI A). In the $B = 0$ case, this time is maximum for electrons with opposite momenta ($\varphi = 0$), which follow time-reversed trajectories. As derived in Ref. 5, in finite *B* the time-reversal symmetry is broken and the maximum interaction time is attained for scattering of electrons with a nonzero angle: $|\varphi| \propto \sqrt{\beta}$. Along with the phase-space argument of Sec. VI A this explains the *B*-*T* scaling mentioned. The low-*B* experimental data of Figs. 4 and 5(a) are in perfect qualitative agreement with these theoretical predictions, strongly supporting our interpretation in terms of the *e*-*e* scattering scenario of Refs. 3 and 5.

The functional *T* and *B* dependencies predicted by expression (3) are weaker than those observed in experiment. Dotted lines in Fig. 4 represent an effort to fit the experimental *B* dependence with expression (3) in the range of magnetic fields where it is applicable. Despite the fact that the overall trends are qualitatively captured by the fits, we observe that a functional *B* dependence in the experiment is appreciably stronger than the theory predicts. Except for the highest $T = 4.2$ K, the empiric dependence of the form $\delta R \propto T^2 B^{-0.7}$ describes the data much better in the same range of *B* (dashed lines in

Fig. 4). The *T* dependence in magnetic field is also somewhat stronger than the theoretical prediction. The dashed line in Fig. 5(b), drawn according to Eq. (3), is not consistent with the experimental dependence (thick solid line) in a typical magnetic field of $B = 15$ mT. At the same time, the empiric dependence $|\delta R(T)| \propto T^{2.5}$ can well describe the data within the experimental uncertainty. Note that the *T* dependence of Fig. 5(b) is discussed in a limited range $T \leqslant 3$ K, which is related to a possible problem with the applicability of the theoretical analysis at high temperatures (see Sec. VI A).

Several possibilities might be responsible for the discrepancy between the theory and experiment in magnetic field. First, we mention the unknown positive *T* dependence of the resistance seen for $|B| \gtrsim 50$ mT (Fig. 3). If additive with the *e*-*e* scattering-induced magnetoresistance at lower $|B|$, such a "wrong-sign" contribution can strengthen the dependence $\delta R(B)$. Second, the T-shaped split-gate layout of our sample (inset to Fig. 1) differs from the theoretical geometry,[5] which might be important for the calculation of the effective interaction times used in the theory. Finally, long-range density gradients around the lateral PC and beam collimation effects discussed in the next subsection can well affect the *e*-*e* scattering contribution in $|B| \neq 0$.

C. Scaling and a_{eff}

As demonstrated in Sec. V, the experimental dependencies $\delta R(B)$ at different R_0 obey scaling in the form $a_{\text{eff}}^{-1}\delta R(B)/R_0 \approx F(a_{\text{eff}}/R_C)$, where the function *F* determines the shape of the *B* dependence at a given temperature. Here we argue that such a scaling is inherent for the *e*-*e* scattering problem in a 2DES in a perpendicular magnetic field.

Consider two classical PCs of widths a_1 and a_2 in magnetic fields corresponding to cyclotron radii of, respectively, R_1 and R_2. Since the phase space for *e*-*e* scattering is determined essentially by the angle between the momenta of scattering electrons, these two problems are similar and can be reduced to each other via scaling of the spatial coordinates, provided $a_1/R_1 = a_2/R_2$. The only difference is that the total scattering probability (proportional to the interaction time) scales as a_i. Hence, we conclude that the *e*-*e* scattering contribution obeys a scaling in the form $a^{-1}\delta G^{ee}/G_0 = F(a/R_C)$. It appears that both analytical expressions of Ref. 5 derived in the limits of low and high β obey such a scaling. This universality is expected to break down only at very low magnetic fields ($R_C \gg l_c$), where a weak disorder scattering comes into play.[5]

As shown in Fig. 6(b), the experimental dependencies $\delta R(B)$ permit scaling of this kind in a wide range of R_0 and all *T* used. This further supports our interpretation of the negative *T* dependence in small *B* in terms of the *e*-*e* scattering mechanism.[5] The scaling also indicates that a problem with a functional dependence $\delta R(B)$, which is appreciably stronger in experiment than in theory, persists regardless of R_0.

As follows from the above argument, the scaling parameter is proportional to the PC half-width *a*. Unexpectedly, the evolution of a_{eff} with R_0 in Fig. 7 is appreciably weaker than that of the physical half-width *a* (symbols and line, respectively). This discrepancy could not be ascribed to experimental uncertainties in scaling procedure and/or evaluation

of a (see Appendix A). The data of Figs. 6(b) and 7 suggest that a different length-scale $\propto a_{\mathrm{eff}}$, rather than a, controls the behavior of the *e-e* contribution to the resistance of a laterally defined PC in a magnetic field. This behavior might be related to a long-range potential landscape nearby the PC, as briefly discussed below.

As a result of stray electric fields from the split gates, an electrostatically defined PC takes the shape of a finite length channel with smooth boundaries. This causes a classical beam collimation effect in lateral PCs.[27] A reduced electron density inside the PC also results in beam collimation via an electrostatic lens effect.[19,28,29] In a model of a horn-shaped channel,[19] the angular dimension of the collimated (injected or incident) electron beam is reduced compared to π. This is compensated for by the increased channel width a_{exit} at the exit (entrance) of the PC, although the conductance G_0 is still given by the minimum channel width a and Eq. (1). Hence, the angular dimension of the PC observed at large distances is increased, $\phi_{\mathrm{PC}} \propto a_{\mathrm{exit}} > a$, which is expected to enhance the relative *e-e* scattering contribution. This effect resembles the operation of a microwave horn antenna. In addition, the collimated beam is squeezed towards the normal to the orifice, so the angular dimension of the orifice is, on average, further increased: $\overline{\phi_{\mathrm{PC}}} \propto \overline{\cos \phi_n}$, where ϕ_n is the angle in respect to the normal to the orifice. Obviously, both effects become more pronounced as the PC is being depleted. One can speculate that, at large l_c, these effects might be roughly described by an extra effective width parameter $a_{\mathrm{eff}} > a$ used instead of a in Eq. (2). Independent experiments could verify whether the results of our scaling procedure in a magnetic field can be interpreted in this way.

D. Evaluation of the interaction parameter α_{ee}

The Coulomb interaction in a 2DES is modified due to screening and correlation effects.[30] *E-e* scattering provides an important information about interactions via a scattering length (cross section in 2D) $\lambda(\theta)$, where θ is a scattering angle.[31] The total scattering probability can be expressed through a total scattering length $\lambda_{\mathrm{tot}} = \int_0^{\pi} \lambda(\theta) d\theta$. In a classical approach of Refs. 3–5 this is determined by a dimensionless interaction parameter α_{ee}: $\lambda_{\mathrm{tot}} = \pi \alpha_{ee}/(4k_F)$. The measurement of the *e-e* scattering contribution to the PC resistance gives a direct access to the scattering length in the 2DES.

Equation (2) permits determination of α_{ee} from the slope of the T dependence at $B = 0$, provided the constriction half-width a and the cutoff length l_c are known. Moreover, analysis of the B dependence of the *e-e* correction allows us to exclude an uncertainty related to the unknown cutoff length l_c, as follows from Eq. (3). However, application of this procedure to the present experiment is problematic due to the discrepancies between theory and experiment discussed above. Still, we attempt to evaluate α_{ee} fitting the zero-field data $\delta R(T)$ by a numerical calculation in spirit of Ref. 3.

As discussed above, at temperatures used in our experiment the estimated mean free path for *e-e* scattering is typically not large compared to the elastic mean free path (and l_c), so the electron beam decay should be taken into account. We employ fits with a numerical calculation, which accounts for the beam

decay on the length scale of the mean free path for the *e-e* scattering. Such fits are capable of describing the data within the whole T range (see Appendix B) and serve as an order of magnitude estimate for α_{ee}.

At a given R_0, the dependence $\delta R(T)/R_0$ from Fig. 2(b) is numerically fitted with three fit parameters a, l_c, and α_{ee}. The best fits are obtained for $l_c = 5$ μm (for $R_0 > 0.64$ kΩ). We used a separate value of $l_c = 8.5$ μm when fitting the lowest PC-resistance data ($R_0 = 0.64$ kΩ), which best reproduces a downturn on the T dependence (see Fig. 12). These values of the cutoff length are substantially smaller than the elastic mean free path in our device ($l_0 \approx 20$ μm). This discrepancy might arise from a crude model used and is not crucial for our purposes. Important for the evaluation of α_{ee} is the knowledge of the parameter a. For a classical PC, a simply equals the half-width of the orifice.[3,5] However, this is not the case in the present experiment for the following reason. In our T-shaped split-gates layout about a half of the electrons can reach the PC after a scattering off the 2DES boundary defined by the right-hand-side gate in the inset of Fig. 1. Assuming a specular boundary scattering, this results in a factor of 2 enhanced a compared to the geometry of Ref. 3 at the same R_0. Therefore, we perform a numerical fit with a equal twice the physical half-width of the PC. We also perform an extra fit using effective width $a = 2a_{\mathrm{eff}}$, as suggested by the scaling of the experimental curves $\delta R(B)$ in a magnetic field.

The interaction constant obtained from such numerical fits is plotted in Fig. 9 as a function of R_0 in the range 0.6 kΩ < R_0 < 3.5 kΩ (symbols). Circles and triangles correspond to fitting with a determined by the physical width and the effective width, respectively. Error bars in the figure indicate an estimated random uncertainty of the evaluation procedure, which is mainly limited by that of the R_0 determination. For each data set α_{ee} is roughly independent of R_0 (exception is the case of $R_0 = 0.64$ kΩ), as expected for the parameter characterizing the strength of the *e-e* scattering in the 2DES. Based on Fig. 9 we conclude that our experiment is consistent with an order of magnitude estimate[3] $\alpha_{ee} \sim 1$. A direct calculation[31] of the 2D scattering length predicts comparable values of the
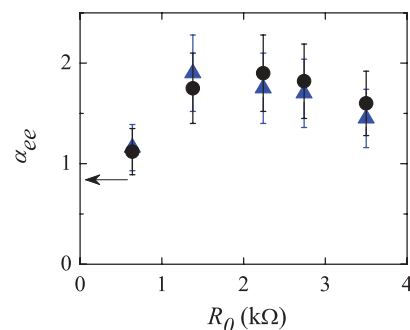

FIG. 9. (Color online) Evaluation of α_{ee} from the zero-field T dependence. Circles and triangles correspond to fitting with a determined by the physical width and the effective width, respectively, as explained in the text. The values of a and a_{eff} used for fitting are shown in Fig. 7 as dots and crosses, respectively. Error bars ($\pm 20\%$) mark the random uncertainty of the evaluation procedure. The arrow points at the value deduced from the calculation[31] of the *e-e* scattering length (see text).

interaction parameter, which increases at decreasing the 2D electron density. We were able to check that at a density of $n_S = 1.5 \times 10^{11}$ cm^{-2}, still almost twice as high as in our 2DES, the calculations[31] predict $\alpha_{ee} \approx 0.84$ (at $T = 2$ K). This value, shown by an arrow in Fig. 9, is roughly consistent with our evaluation. Unfortunately, a systematic uncertainty, associated with our fitting procedure and large number of fit parameters, by far exceeds the random uncertainty in Fig. 9. This does not permit a quantitative comparison beyond an order of magnitude estimate. The data of Fig. 9 is rather meant to illustrate that, in a wide range of R_0, the absolute value $\delta R(T)$ is roughly consistent with the predictions of the *e-e* scattering scenario.

VII. SUMMARY

In summary, we studied a T-dependent contribution δR to the resistance of a ballistic PC in a 2DES of a high-quality GaAs/AlGaAs heterostructure at temperatures below 4.2 K. In zero magnetic field, the resistance decreases by ~10–20% as the temperature is raised from 0.5 K to 4.2 K. The dependence is roughly linear below 2 K and weakens at higher T. A B-driven suppression of δR is found in perpendicular magnetic fields of a few 10 mT and not too high T. These results give strong evidence for the influence of the *e-e* scattering on the PC conductance. The observations are similar in a wide range of R_0, even outside the classical PC regime, and can be qualitatively described with the *e-e* scattering scenario of Refs. 3 and 5. We argue that in the $B = 0$ case the discrepancies between the experiment and theory can be well understood and supported by a numerical calculation. In a magnetic field, the curves $\delta R(B)$ permit single-parameter scaling in a wide range of PC resistances R_0, which is an intrinsic property of the *e-e* scattering problem. Contrary to expectations, the dependence of the scaling parameter on R_0 is sufficiently weaker than that of the physical half-width of the orifice. This indicates that the value of the *e-e* scattering contribution in a lateral PC is determined by an independent parameter a_{eff}, which we call an effective half-width of the PC. In the $B = 0$ case, we perform a numerical calculation, which goes beyond theoretical assumptions[3] and is capable of quantitatively describing the experimental data in the whole temperature range. Using this calculation, the interaction constant α_{ee} of the 2DES is evaluated, which is in rough quantitative agreement with the calculations[31] of the *e-e* scattering length in 2DESs in GaAs.

APPENDIX A: EVALUATION OF THE ELECTRON DENSITY INSIDE THE PC

The resistance R_0 of a quasiclassical PC and its physical half-width a (at a Fermi level) are directly related as $R_0 \propto C_1/(ak_F^{\text{PC}})$, where the Fermi wave-vector is given by $k_F^{\text{PC}} = (2\pi n^{\text{PC}})^{1/2}$ and n^{PC} is the (2D) electron density inside the PC. The numerical coefficient depends on the model of the confinement potential and equals $C_1 = \pi$ (4), respectively, for a hard-wall (parabolic) confinement. Separate determination of a and n^{PC} is possible by analyzing the depopulation of the magnetoelectric subbands in a perpendicular magnetic field.

The depopulation effect gives rise to a positive contribution to the magnetoresistance of the quasiclassical PC, which to the lowest order in B is given by[19]

$$\frac{\delta R_{\text{depop}}}{R_0} = C_2 \left(\frac{a}{R_C^{\text{PC}}}\right)^2 \propto (C_1)^2 C_2 \frac{B^2}{(n^{\text{PC}})^2}, \qquad \text{(A1)}$$

where $R_C^{\text{PC}} = k_F^{\text{PC}} \hbar c (eB)^{-1}$ is the cyclotron radius corresponding to the electron density inside the PC. The confinement model-dependent coefficient equals $C_2 = 1/6$ (1/2), respectively, for a hard-wall (parabolic) confinement. Here we also used $a \propto C_1/k_F^{\text{PC}}$, since R_0 is fixed. The evaluated density depends on the details of the PC confinement via a factor $C_1(C_2)^{1/2}$ equal to $\approx$1.28 (2.83) for a hard-wall (parabolic) model confinement potential. In fact, a gradual transition from a hard-wall-like confinement in a wider constriction to a parabolic-like confinement in a narrower constriction is typically found[32] in agreement with numerical simulations (see Ref. 19 for references). Here, we evaluate the electron density n^{PC} assuming a hard-wall confinement with the help of Eq. (2.62a) of Ref. 19. In this way a lower boundary for n^{PC} is obtained and the strongest possible gate-voltage dependence of the electron density inside the PC.

The result is shown in Fig. 10 for gate voltages in the range corresponding to 0.64 kΩ $\leqslant R_0 \leqslant$ 3.5 kΩ (symbols). Here, the lowest T experimental data were used, where the
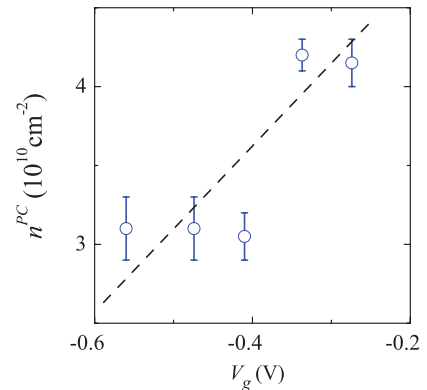

FIG. 10. (Color online) Evaluation of the electron density inside the PC from subband depopulation effect, assuming a hard-wall confinement. Experimental points for a set of gate voltages are shown by symbols. These symbols indicate values of the density averaged over several experiments at the same V_g. Error bars represent a random uncertainty, which comes from both the accuracy of the fits and the reproducibility of the magnetoresistance traces $R(B)$. The dashed line is the best linear fit $\delta n^{\text{PC}} \propto \delta V_g$.

contribution of the *e-e* scattering to the magnetoresistance is not important (see Sec. IV). The evaluated density n^{PC} is reduced by at least a factor of 2 compared to that in the bulk 2DES and further decreases towards the lower V_g. Note that assuming a parabolic confinement would result in factor of 2.2 higher density that is pretty close to the bulk 2DES value ($n_S \approx 0.83 \times 10^{11}$ cm^{-2}). Most probably, the actual density is somewhere in between the two limiting cases.

Strictly speaking, the data scatter in Fig. 10 precludes an accurate evaluation of the gate-voltage dependence of n^{PC}. As a crude estimate, we take the simplest capacitive approximation $\delta n^{PC} \propto \delta V_g$ to describe the data, which is reasonable for a relatively deep 2DES used. The dashed line is the best linear fit extrapolating to $n^{PC} = 0$ near the pinch-off point of the PC at $V_g \approx -1.1$V. It is this fit that was used for the evaluation of the physical half-width a in Fig. 7. Note that an $\approx 16\%$ uncertainty in a, associated with the confinement model choice ($a \propto C_1^{1/2} C_2^{-1/4}$), is not crucial for us (see Fig. 9). At the same time, an account of a gradual change from a hard-wall-like to a parabolic-like confinement at decreasing V_g could only cause a functional dependence of $a(R_0)$ in Fig. 7 to become further from $a_{\text{eff}}(R_0)$.

APPENDIX B: NUMERICAL CALCULATION

We perform a numerical calculation of the *e-e* scattering contribution in a 2DES for $B = 0$ in the spirit of Ref. 3. This task involves a six-dimensional integration,

$$\frac{\delta G}{G_0} = \frac{\alpha_{ee} k_F a}{8\pi^2} \int_0^{\pi/2} \cos\phi_p d\phi_p \int_1^{l_c/a} dr \int d\phi_k \int d\theta$$
$$\times \iint \frac{f_{p'} f_{k'} + f_p - f_p f_{p'} - f_p f_{k'}}{T \cosh^2 \frac{\varepsilon_k - 1}{T}} d\varepsilon_p d\varepsilon_k. \quad \text{(B1)}$$

Here p, ε_p (k, ε_k) is the momentum and energy (in units of E_F) of the electron incident to (injected through) the PC orifice, respectively. After scattering the electrons acquire the momenta p' and k'. The angle of p in respect to the direction normal to the orifice is denoted as ϕ_p; ϕ_k is the angle between the direction towards the center of the orifice and momentum k; θ is the scattering angle in the relative momentum space. The distance r from the PC is measured in units of PC half-width a (region $r < a$ is omitted) and the temperature T in units of E_F. The equilibrium distribution functions for the momenta p, p', k' are denoted by $f_p, f_{p'}, f_{k'}$. In this expression we accounted for the energy and momentum conservation laws and substituted the distribution f_k by its nonequilibrium part linearized in respect to bias voltage across the PC. Integration over ϕ_k is restricted to the angular dimension of the electron beam injected through the PC $\phi_k \in (-\phi_{\text{max}}, \phi_{\text{max}})$, where $\phi_{\text{max}} = \arctan(\cos\phi_p/r)$. Integration over θ is limited to the scattering angles such that electrons k' and p' do not reach the orifice. At a given T we restrict the integration over electrons' energies to the interval $E_F \pm 5T$.

In Fig. 11 we plot the results of the numerical calculation for $\alpha_{ee} = 1, a = 400$ nm and a set of l_c values between 5 μm and 100 μm. We find that at high T the slope of the T dependence is approximately proportional to $\ln(l_c/a)$, in agreement with the analytic result of Eq. (2). To illustrate this, for each l_c the calculated relative contribution $\delta G/G_0$ was divided by
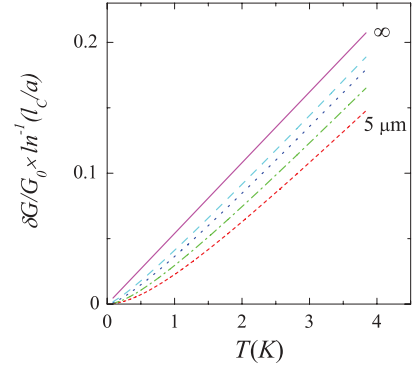

FIG. 11. (Color online) Results of a numerical calculation of the *e-e* scattering contribution in a zero magnetic field. The data correspond to $\alpha_{ee} = 1, a = 400$ nm and a set of $l_c = \infty, 100, 30, 10, 5$ μm from top to bottom curve. The ordinate axis is chosen to illustrate the dependence on l_c; see text.

$\ln(l_c/a)$ in Fig. 11 to give approximately the same slope at high T. In the limiting case $l_c \to \infty$ we recover the result of Eq. (2), although the numerical coefficient obtained is a factor of ≈ 1.7 larger. The origin of this discrepancy is unclear and we compensate for this when fitting the experimental data.

With increasing T a mean free path l_{ee} for the *e-e* scattering decreases and eventually becomes comparable to or smaller than the cutoff length scale $l_c \sim l_0$. This means that an electron beam injected through the PC decays at a typical distance of l_{ee} from the PC orifice. In order to numerically estimate the *e-e* scattering contribution to the PC resistance in this regime we weight the integral over the dimensionless distance r in (B1) by an exponential factor $\exp(-ar/l_{ee})$, where the T-dependent l_{ee} is taken from the quasiparticle lifetime calculations.[24] Most probably, this approach cannot be justified by a solution of the kinetic equation and should be treated as a first crude step on the way to a self-consistent calculation. Nevertheless, such an account of the beam decay allows us to describe the experimental T dependence in the whole range of temperatures. In Fig. 12
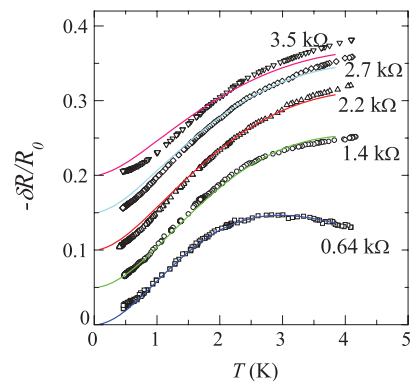

FIG. 12. (Color online) Normalized experimental T dependence of the PC resistance (symbols) together with numerical fits accounting for the beam decay effect (lines), shifted in steps of 0.05 along the ordinate axis for clarity. These fits are obtained with the cutoff length equal to $l_c = 8.5$ μm for $R_0 = 0.64$ kΩ and $l_c = 5$ μm for the four other curves. The parameter a equals twice the physical half-width of the PC orifice from Fig. 7 (dots). The *e-e* interaction parameter values are given in Fig. 9 (circles).

we plot the best numerical fits (lines) to the experimental data (symbols) for the five lowest values of R_0 used. The data ordinate are shifted in steps of 0.05 for successive R_0. The saturation of the T dependence in the range $T > 2$ K is perfectly reproduced by the fits, which strongly supports our interpretation in terms of the e-e scattering. The overall quality of the fits is pretty good for $R_0 \leqslant 2.7$ kΩ. At higher R_0 the agreement is worse, presumably thanks to a residual thermal smearing of the conductance plateaus (see Sec. III).

As follows from Figs. 11 and 12, a cutoff length on the order of $l_c \sim 10$ μm is too small to clearly observe the proportionality[3] $\delta G_{ee} \propto T$. Improving the sample quality, one could achieve a longer elastic mean free path (and l_c), which favors linearity of the T dependence at temperatures such that $T/E_F \gg a/l_c$ (see Fig. 11 and discussion in Sec. VI A). On the other hand, the beam decay effect could not be neglected unless $l_c \ll l_{ee}$, which is harder to satisfy at higher l_c. The trade-off is to increase l_c and measure at lower temperatures in order to satisfy simultaneously $a(T/E_F)^{-1} \ll l_c \ll l_{ee} \propto (T/E_F)^{-2}/\ln(E_F/T)$. These conditions are possible, yet challenging, to meet and are simpler to do in higher-density (large E_F) samples. For GaAs, we expect that a T dependence close to $\delta G_{ee} \propto T$ could be observed at 0.1 K $< T <$ 1 K in samples with a 2DES mobility exceeding 10^7 cm^2/Vs.

---

[1] Yu. V. Sharvin, Zh. Eksp. Teor. Fiz. **48**, 984 (1965) [Sov. Phys. JETP **21**, 655 (1965)]; Yu. V. Sharvin and N. I. Bogatina, Zh. Eksp. Teor. Phys. **56**, 772 (1969) [Sov. Phys. JETP **29**, 419 (1969)].

[2] L. I. Glazman, G. B. Lesovik, D. E. Khmelnitskii, and R. I. Shekhter, JETP Lett. **48**, 238 (1988).

[3] K. E. Nagaev and O. S. Ayvazyan, Phys. Rev. Lett. **101**, 216807 (2008).

[4] K. E. Nagaev, T. V. Krishtop, N. Yu. Sergeeva, Pis'ma v ZhETF **94**, 53 (2011).

[5] K. E. Nagaev and T. V. Kostyuchenko, Phys. Rev. B **81**, 125316 (2010).

[6] B. J. van Wees, H. van Houten, C. W. J. Beenakker, J. G. Williamson, L. P. Kouwenhoven, D. vander Marel, and C. T. Foxon, Phys. Rev. Lett. **60**, 848 (1988).

[7] D. A. Wharam, T. J. Thornton, R. Newbury *et al.*, J. Phys. C **21**, L209 (1988).

[8] P. F. Bagwell and T. P. Orlando, Phys. Rev. B **40**, 1456 (1989).

[9] B. J. van Wees, L. P. Kouwenhoven, E. M. M. Willems, C. J. P. M. Harmans, J. E. Mooij, H. van Houten, C. W. J. Beenakker, J. G. Williamson, and C. T. Foxon, Phys. Rev. B **43**, 12431 (1991).

[10] K. J. Thomas, J. T. Nicholls, M. Y. Simmons, M. Pepper, D. R. Mace, and D. A. Ritchie, Phys. Rev. Lett. **77**, 135 (1996).

[11] L. W. Molenkamp and M. J. M. de Jong, Phys. Rev. B **49**, 5038 (1994); M. J. M. de Jong and L. W. Molenkamp, *ibid.* **51**, 13389 (1995).

[12] R. N. Gurzhi, A. N. Kalinenko, and A. I. Kopeliovich, Phys. Rev. Lett. **74**, 3872 (1995).

[13] A. O. Govorov and J. J. Heremans, Phys. Rev. Lett. **92**, 026803 (2004).

[14] D. Taubert, G. J. Schinner, H. P. Tranitz, W. Wegscheider, C. Tomaras, S. Kehrein, and S. Ludwig, Phys. Rev. B **82**, 161416(R) (2010); D. Taubert, C. Tomaras, G. J. Schinner, H. P. Tranitz, W. Wegscheider, S. Kehrein, and S. Ludwig, *ibid.* **83**, 235404 (2011).

[15] V. T. Renard, O. A. Tkachenko, V. A. Tkachenko, T. Ota, N. Kumada, J. C. Portal, and Y. Hirayama, Phys. Rev. Lett. **100**, 186801 (2008).

[16] N. K. Patel, J. T. Nicholls, L. Martín-Moreno, M. Pepper, J. E. F. Frost, D. A. Ritchie, and G. A. C. Jones, Phys. Rev. B **44**, 13549 (1991).

[17] M. Büttiker, Phys. Rev. B **41**, 7906 (1990).

[18] See Supplemental Material at http://link.aps.org/supplemental/10.1103/PhysRevB.86.075425 for (i) examples of conductance quantization in one of our devices (Fig. 1) and (ii) a plot of parameters R_0 along with the T dependence (Fig. 2).

[19] C. W. J. Beenakker and H. van Houten, Solid State Phys. **44**, 1 (1991).

[20] H. van Houten, C. W. J. Beenakker, P. H. M. vanLoosdrecht, T. J. Thornton, H. Ahmed, M. Pepper, C. T. Foxon, and J. J. Harris, Phys. Rev. B **37**, 8534 (1988).

[21] A sharp $B = 0$ kink of the dashed line in the inset of Fig. 3(a) is a property of an idealized 2DES. A finite elastic mean free path of $l_0 \approx 20$ μm in our device is believed to result in a rounding of the kink in magnetic fields of a few mT, where the cyclotron radius exceeds l_0.

[22] This behavior in magnetic fields is in stark contrast with that of a well-known weak-localization (WL) correction in diffusive 2D and quasi-1D systems. In those systems, the low-B magnetoresistance is (i) negative and (ii) strengthens at decreasing T (see, e.g., Ref. 25 and Ref. 19 for a review), which is opposite to our observations. Obviously, the WL physics is not important in clean ballistic PCs we study here.

[23] At $T \to 0$ we expect instead of Eq. (2) a simpler relation $\delta G_{ee}/G_0 \sim l_c/l_{ee}^* \ll 1$, where $l_{ee}^* \propto T^{-2}$ is a mean free path for e-e scattering in the 2DES, determined by large-angle scattering.[12] Note, however, that in this limit the notion of the cutoff length l_c may be incorrect (K. E. Nagaev, private communication).

[24] G. F. Giuliani and J. J. Quinn, Phys. Rev. B **26**, 4421 (1982).

[25] K. K. Choi, D. C. Tsui, and K. Alavi, Phys. Rev. B **36**, 7751 (1987).

[26] B. J. LeRoy, J. Phys.: Condens. Matter **15**, R1835 (2003).

[27] L. W. Molenkamp, A. A. M. Staring, C. W. J. Beenakker, R. Eppenga, C. E. Timmering, J. G. Williamson, C. J. P. M. Harmans, and C. T. Foxon, Phys. Rev. B **41**, 1274 (1990).

[28] U. Sivan, M. Heiblum, C. P. Umbach, and H. Shtrikman, Phys. Rev. B **41**, 7937 (1990).

[29] J. Spector, H. L. Stormer, K. W. Baldwin, L. N. Pfeiffer, and K. W. West, Appl. Phys. Lett. **56**, 1290 (1990).

[30] F. Stern, Phys. Rev. Lett. **18**, 546 (1967).

[31] D. S. Saraga, B. L. Altshuler, D. Loss, and R. M. Westervelt, Phys. Rev. B **71**, 045338 (2005).

[32] D. A. Wharam, U. Ekenberg, M. Pepper, D. G. Hasko, H. Ahmed, J. E. F. Frost, D. A. Ritchie, D. C. Peacock, and G. A. C. Jones, Phys. Rev. B **39**, 6283 (1989).